Ultrasmall and Ultralow Threshold GaInAsP–InP Microdisk Injection Lasers: Design, Fabrication, Lasing Characteristics, and Spontaneous Emission Factor

Masayuki Fujita, Atsushi Sakai, and Toshihiko Baba, *Member, IEEE*

***Abstract*— We have calculated lasing characteristics of current injection microdisk lasers of several microns in diameter, taking account of the scattering loss at center posts and the carrier diffusion effect. We found that the optimum width of the disk wing exposed to the air is 0.6–0.7 μm and the minimum threshold current is nearly 10 μA for the disk diameter of 2 μm. The internal differential quantum efficiency can be 95% if the transparent carrier density is reduced to 7.5×10^{17} cm^{-3} and the diffusion constant is increased to 8 cm^2/s. In the experiment, we have obtained the room temperature continuous-wave operation of a GaInAsP–InP device of 3 μm in diameter, for the first time, with a record low threshold of 150 μA. This achievement was mainly owing to the reduction of the scattering loss at the disk edge, and hence the reduction of the threshold current density. The spontaneous emission factor was estimated to be 6×10^{-3}. This value was much reduced by the large detuning of the lasing wavelength against the spontaneous emission peak. A larger value over 0.1, which is expected for such a small device, will be obtained by the wavelength tuning and the narrowing of the spontaneous emission spectrum.**

***Index Terms*— FDTD, GaInAsP–InP, microcavity, microdisk, semiconductor laser, spontaneous emission control, whispering gallery mode.**

I. Introduction

MICROCAVITY lasers have possibilities of an ultralow threshold due to the small volume of the active region and a large spontaneous emission factor due to the small volume of the cavity [1]–[3]. Especially, in these ten years, much attention have been directed to the ultimate reduction of the cavity volume with maintaining a high quality factor Q. Such an ultrasmall cavity is expected to provide the thresholdless operation by the perfect single mode condition that only one mode is allowed in the spontaneous emission spectrum. Microdisks are promising candidates that achieve such cavities due to the simple geometry and the simple fabrication process. The lasing in photo-pumped devices has been demonstrated for various compound systems [4]–[9]. The diameter of a GaInAsP–InP device has been reduced to 1.6 μm and the spontaneous emission factor has been roughly estimated to be 0.2 by counting the number of resonant modes in the spontaneous emission spectrum [10]. However, it is difficult to discuss actual applications of photo-pumped devices at this stage, since the pump efficiency is impractically low. The lasing in current injection devices has been demonstrated only for GaInAsP–InP [11] and GaInAs–AlInAs [12] systems. This seems to be due to the more complex structures and the more difficult measurement than those of photopumped devices. For a GaInAsP–InP device, we have reduced the disk diameter to 2 μm and demonstrated a low threshold lasing at room temperature by using a microprobe measurement [13]. However, all the lasing so far reported for current injection devices were under pulsed condition; although the pulsed threshold current is typically lower than 1 mA, the continuous-wave (CW) operation has never been obtained. It has been suggested in the experiment that a large thermal resistance of the order of 10^5 K/W disturbed the CW operation [3]. Owing to the growing interest for the spontaneous emission factor in microcavity lasers, the theoretical behavior of modes in microdisks has often been discussed. However, the mode behavior below threshold is difficult to evaluate precisely under pulsed condition, so that the spontaneous emission factor has never been evaluated for current injection devices. On the contrary, the improvement of lasing characteristics themselves has not been discussed at all.

Fig. 1 illustrates the schematic of a current injection device. The center of the circular disk active layer is supported by upper and lower posts. Whispering gallery (WG) modes round near the disk edge, repeating the total reflection at semiconductor/air boundaries. The current is flowed from the top contact and carriers are injected into the active layer from the posts. WG modes acquire the optical gain by the carrier diffusion to the disk edge and the lasing operation occurs. Normally, cross-sections of posts formed by a selective wet etching are square due to the anisotropy of the etching, as indicated in Fig. 1(a). Therefore, larger posts cause the serious scattering loss of WG modes, while smaller posts cause the insufficient carrier diffusion, resulting in the nonumiform optical gain. In this study, we calculated the scatting loss at posts using the finite-difference time-domain (FDTD) method [14] and lasing characteristics from rate equations including

Manuscript received November 30, 1998; revised April 12, 1999. This work was supported in part by the Ministry of Education, Science, Sports, and Culture and the Support Center for Advanced Telecommunications Technology Research under Grant-in-Aid 10450025, and in part by the Japan Society for Promotion of Science, Research for the Future, under Grant JSPS-RFTF 97P00103.

The authors are with the Division of Electrical and Computer Engineering, Yokohama National University, Hodogayaku, Yokohama 240-8501, Japan.

Publisher Item Identifier S 1077-260X(99)05356-3.

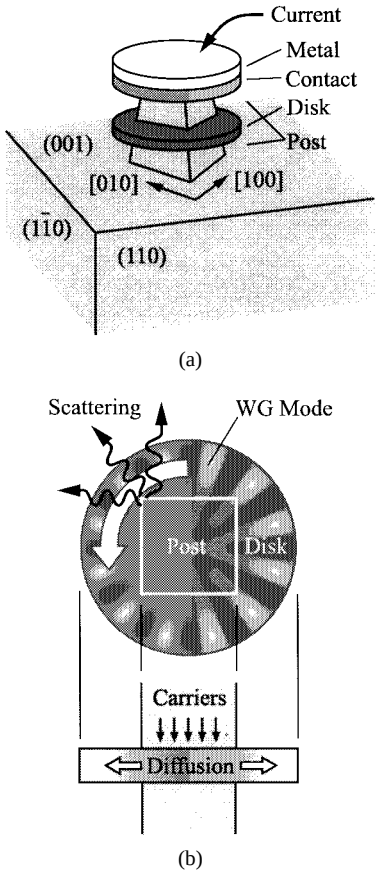

Fig. 1. Schematic of microdisk injection laser. (a) Overview. (b) Topview and sideview.

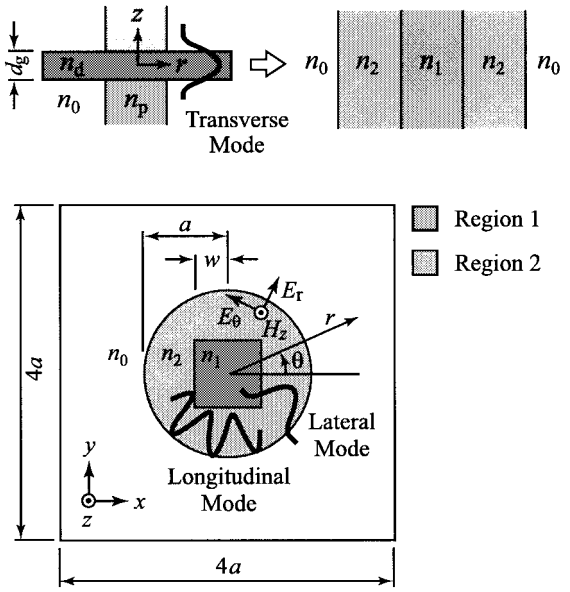

Fig. 2. 2-D FDTD calculation model with equivalent refractive index approximation and coordinate system.

TABLE I
PARAMETERS USED IN FDTD CALCULATION OF WG MODES AND SCATTERING LOSS AT POSTS

$n_d = 3.39$	$n_p = 3.17$	$n_0 = 1.0$
$d_g = 0.2\,\mu m$	$n_1 = 3.20$	$n_2 = 2.65$
$A = 1000$	$m_0 = 5000$	$\sigma = 0.025\omega_0$
$\Delta t = 0.025$ fs	$\Delta x = 12.5$ nm	$\Delta y = 12.5$ nm
$2a = 2\,\mu m$		$2a = 3\,\mu m$
$\lambda_0 = 1.54\,\mu m$		$\lambda_0 = 1.52\,\mu m$

the carrier diffusion effect [15]. We designed the optimum structure from these results. In addition, we improved the fabrication process of GaInAsP–InP current injection devices and achieved the room temperature CW operation, for the first time, with a record-low threshold of 150 μA. Also, we evaluated the spontaneous emission factor of this device by the curve fitting method [16].

In this paper, the calculation and the design will be presented in Section II, the fabrication process and lasing characteristics in Section III, and the discussion on the spontaneous emission factor in Section IV.

II. Analysis and Design

A. Scattering Loss by Posts

Fig. 2 shows the calculation model and the coordinate system. The device structure is separated by two regions concerned with the waveguide structure in the z direction, i.e., Region 1 in which the disk is supported by posts, and Region 2 in which the disk is exposed to the air. For simple calculation, the three-dimensional (3-D) structure was simplified to a two-dimensional (2-D) model in the xy plane using equivalent refractive indexes of transverse modes in waveguides. The equivalent index n_1 of Region 1 was calculated from the thickness of the disk d_g, the average index of the disk n_d, and the index of posts n_p using the simple waveguide analysis. Similarly, the equivalent index n_2 of Region 2 was calculated from d_g, n_d and the index of the outer space n_0. Each side of the model was set to be twice the disk diameter. The Mur's second order absorbing condition [17] was used as the boundary condition on the peripheries of the model. The polarization was fixed to the transverse electric (TE) whose electric field vector lies inside the xy plane. This assumption well simulates the polarization anisotropy of the spontaneous emission from the compressive-strained multiquantum-wells (CS-MQW) used in the experiment. The initial excitation was given for the magnetic field of a cell near the edge inside the disk with the time-dependent function $H_z = A\cos[\omega_0(m-m_0)\Delta t]\exp\lfloor -\{\sigma(m-m_0)\Delta t\}^2/2\rfloor$, where A is the amplitude, ω_0 the center angular frequency of the excitation, m the time step, m_0 the delay step of the pulse peak, σ the spectral broadening factor, and Δt the time interval between steps. Δt was determined from the condition $\Delta t < c^{-1}[(\Delta x)^{-2} + (\Delta y)^{-2}]^{-1/2}$, where c is the vacuum velocity of light, and Δx and Δy are cell sizes. The center wavelength of the excitation λ_0 is related to ω_0 as $\lambda_0 = 2\pi c/\omega_0$. It was selected close to the analytical solution of the resonant wavelength of a WG mode to excite this mode efficiently within small steps. The unit cell dividing the model is a square, $\lambda_0/(40n_1)$ on a side. This size is small enough to obtain the resonant wavelength within 1% error [18].

Parameters assumed in the calculation are summarized in Table I. They are typical for 1.55-μm-GaInAsP–InP CS-MQW

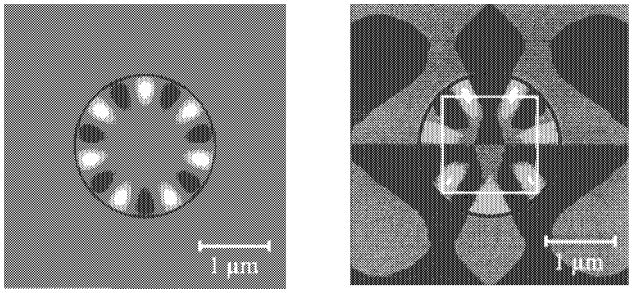

(a) (b)

Fig. 3. Magnetic field distribution of WG mode H_z for $2a = 2$ μm. (a) Without posts ($w = 0$ μm). (b) With posts (0.7 μm).

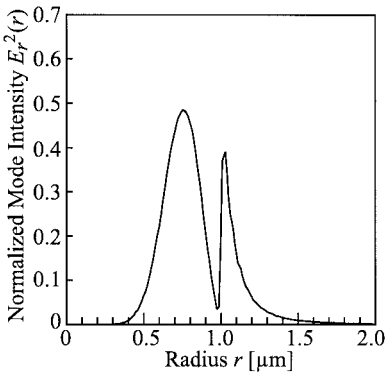

(a)

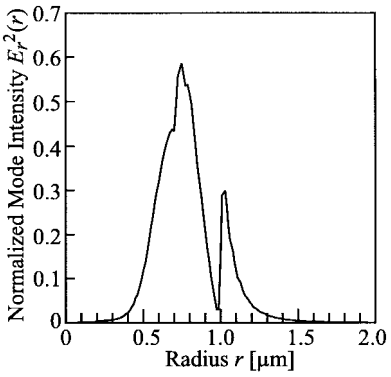

(b)

Fig. 4. Normalized mode intensity $E_r^2(r)$ for $2a = 2$ μm. (a) Without posts ($w = 0$ μm). (b) Wth posts (0.7 μm).

wafer at room temperature. Electromagnetic fields E_r, E_θ, and H_z were calculated up to $m = 2^{17}$, at which the excitation function is negligibly small and only one WG mode is left behind inside the disk. Fig. 3 shows examples of the magnetic field distribution of a WG mode H_z when the disk diameter $2a$ is 2 μm. It is seen from the comparison between the disk with and without posts that the field distribution is strongly affected by post edges. Fig. 4 shows the mode intensity $E_r^2(r)$ which is given by taking an average with respect to the angle θ and normalizing so that $\int_0^\infty E_r^2(r) 2\pi r\, dr = 1$. From the small mode intensity at $r \leq 0.4$ μm, it is expected that the influence of posts is small when $w \leq 0.4$ μm.

The Q factor is defined as $Q = \omega W/P$, where W is the energy stored in the disk and P is the power radiated outside

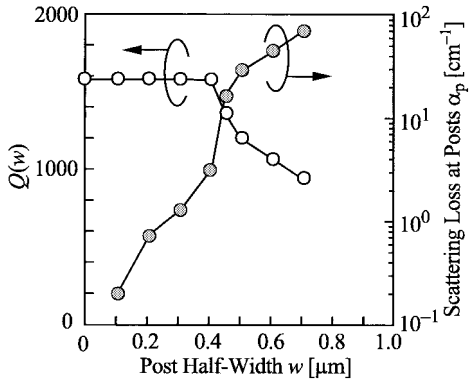

Fig. 5. Cavity Q and scattering loss α_p calculated with post half-width w for $2a = 2$ μm.

the disk. The scattering loss by posts α_p is given by

$$\alpha_p = \frac{2\pi}{\lambda_r} n_{eq} \left[\frac{1}{Q(w)} - \frac{1}{Q(0)} \right] \tag{1}$$

where λ_r is the resonant wavelength, n_{eq} is the equivalent index of the WG mode, and $Q(w)$ denotes the Q factor as a function of the half-width of posts w. The index n_{eq} can be almost approximated by n_2, since the WG mode considered here is almost localized in Region 2. Fig. 5 shows $Q(w)$ and α_p calculated with the half-width w. For $w \leq 0.4$ μm, $Q(w)$ is nearly 1600 and constant. This value is not dominated by the scattering loss at posts α_p but by the scattering at the disk edge α_s. The scattering loss α_s is automatically introduced in the FDTD calculation, since the finite cell size can only simulate a disk edge with roughness. An ideal Q value for a perfectly smooth disk with no pedestals and absorption is analytically obtained to be of the 10^5 order. However, such a high Q was not obtained by the FDTD calculation even though the cell size was reduced to as small as $\lambda_0/(80n_1)$. Further reduction of the cell size may increase the Q value to some extent. However it was restricted by the computer resource used in this study. So, we evaluated α_p from the relative change of $Q^{-1}(w)$ against $Q^{-1}(0)$, as expressed in (1). Therefore, in contrast to $Q(w)$, the change of α_p in Fig. 5 is gradual over $w = 0$–0.7 μm. For $w > 0.4$ μm, α_p exceeds 5 cm^{-1}. This value $\alpha_p > 5$ cm^{-1} is serious for lasing characteristics since it is comparable to or even larger than other cavity losses.

B. Lasing Characteristics

In the FDTD calculation in Section II-A, square cross-sections of posts were taken into account. However, the distribution of the mode intensity was averaged with respect to the angle θ. Here, we average the square shape itself with respect to θ to simplify rate equations for the static condition as

$$\begin{aligned} &(\text{Region 1: } 0 \leq r \leq r_1) \\ &\quad 0 = \left[-G(N(r)) E_r^2(r) \Gamma_{z1} \pi a^2 \right] S \\ &\qquad - \left[BN^2(r) + C_A N^3(r) \right] \\ &\qquad + D \left[\frac{1}{r} \frac{dN(r)}{dr} + \frac{d^2 N(r)}{dr^2} \right] + \left[\frac{I}{e_0 \pi r_1^2 d_w} \right] \end{aligned} \tag{2}$$

(Region 2: $r_1 \le r \le a$)

$$0 = \left[-G(N(r))E_r^2(r)\Gamma_{z2}\pi a^2\right]S - \left[BN^2(r) + C_A N^3(r)\right] + D\left[\frac{1}{r}\frac{dN(r)}{dr} + \frac{d^2N(r)}{dr^2}\right] \quad (3)$$

(Regions 1 and 2: $0 \le r \le a$)

$$0 = \left[\int_0^{r_1} G(N(r))E_r^2(r)\Gamma_{z1}2\pi r\,dr + \int_{r_1}^{a} G(N(r))E_r^2(r)\Gamma_{z2}2\pi r\,dr\right]S - \frac{S}{\tau_p} + \left[C_1\int_0^{r_1} BN^2(r)E_r^2(r)2\pi r\,dr + C_2\int_{r_1}^{a} BN^2(r)E_r^2(r)2\pi r\,dr\right] \quad (4)$$

where $N(r)$ is the carrier density, S the photon density of the lasing mode, $G(N(r))$ the gain coefficient, Γ_{z1} and Γ_{z2} the confinement factor of the transverse mode into the active layer in Regions 1 and 2, respectively, B the radiative recombination coefficient, C_A the Auger recombination coefficient, D the diffusion constant, I the injection current, e_0 the electron charge, d_w the total thickness of quantum-wells, r_1 the average distance from the center to the edge of posts, and τ_p the photon lifetime. The radius r_1 is nearly 1.12 times the half-width of posts w. Factors C_1 and C_2 are related to the spontaneous emission factor C as $C_i = [\Gamma_{zi}/(\Gamma_{z1}\Gamma_{xy1} + \Gamma_{z2}\Gamma_{xy2})]C$, where $i = 1$ or 2. Γ_{xy1} and Γ_{xy2} are the confinement factors of the lateral mode in Regions 1 and 2, respectively. In the calculation, they were approximated by

$$\Gamma_{xy1} = \int_0^{r_1} E_r^2(r)2\pi r\,dr$$
$$\Gamma_{xy2} = \int_{r_1}^{a} E_r^2(r)2\pi r\,dr. \quad (5)$$

In (2), the uniform carrier injection into Region 1 is assumed. The stimulated emission for nonlasing modes was ignored, since Q factors of nonlasing modes rounding inside the disk are much lower than that of the lasing mode due to the scattering loss at post edges. The third term in the right side of (2) and (3) denotes the carrier diffusion effect. Boundary conditions at the center and the disk edge are

$$\left.\frac{dN(r)}{dr}\right|_{r=0} = 0 \quad (6)$$

$$e_0 N(a) v_s = -e_0 D \left.\frac{dN(r)}{dr}\right|_{r=a} \quad (7)$$

respectively, where v_s is the surface recombination velocity. We applied (6) and (7) to (2)–(4), and then transformed into the finite difference formula. Solving these equations by the Newton–Rapson method, we obtained $N(r)$, S, the threshold current I_{th} and the internal differential quantum efficiency $\eta_{di} \equiv \partial[S/\tau_p]/\partial[I/e_0(\pi r_1^2)\,d_w]$.

Parameters used in the caluculation are summarized in Table II. They are also typical for GaInAsP–InP CS-MQW wafer at room temparature. The diffusion constant D is determined by the mobility of electrons μ_e, that of holes μ_h and the electrical neutral condition [19]; when $\mu_e = 3000$ cm^2/V·s and $\mu_h = 20$–300 cm^2/V·s are assumed, D is calculated to be 1–14 cm^2/s. Considering the CS-MQW, the logarithmic gain $G(N) = G_0(c/n_{eq})\ln(N/N_0)$ was assumed [20], where N_0 is the carrier density for the transparency and G_0 is the differential gain at $N = N_0$. They were evaluated, as shown in Table II, for broad-area lasers fabricated into the same wafer as used in this experiment. The photon lifetime τ_p is expressed as $\tau_p = n_{eq}/(c\alpha)$, where α is the total cavity loss given by the sum of the internal absoption loss α_a, the scattering loss at the disk surface and egde α_s, the scattreing loss at posts α_p, and the diffraction loss for the disk without posts α_d. Now, we consider an ideal structure so that $\alpha_s = 0$ cm^{-1}. The internal absoption loss α_a was evaluated to be 5 cm^{-1} for broad-area lasers. The scattering loss α_p depends on the width w, as shown in Section II-A. It has been reported that the diffraction loss α_d caluculated by the 2-D FDTD method with the equivalent index approximation is much larger than that expected in a 3-D disk stracture [21]. Thus, the approximate expression derived for 3-D structures by the WKB method was used to evaluated α_d [4]. The radiative recombination coefficient B was evaluated from the carrier lifetime for broad-area lasers and modified by the assumption that it is proportional to n_{eq} [22]. The C factor was caluculated from the experssion shown in Section IV, assuming that the detuning of the resonant wavelength against the spontaneous emission peak was zero.

TABLE II
PARAMETERS USED IN RATE EQUATION ANALYSIS

$\Gamma_{z1} = 2.8$ %	$\Gamma_{z2} = 7.9$ %	$d_w = 16$ nm
$v_s = 1\times10^4$ cm/s	$B = 1.6\times10^{-10}$ cm^3/s	$C_A = 5.0\times10^{-29}$ cm^6/s
$G_0 = 1500$ cm^{-1}	$N_0 = 1.5\times10^{18}$ cm^{-3}	

$2a = 2$ μm	$2a = 3$ μm
$C = 0.19$	$C = 0.10$
$\alpha_d = 0.19$ cm^{-1}	$\alpha_d = 9.8\times10^{-5}$ cm^{-1}

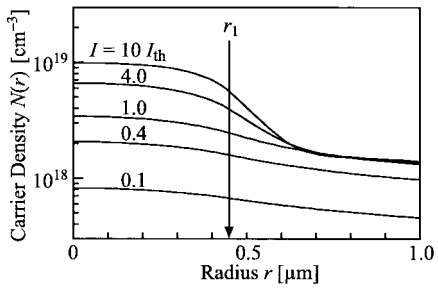

Fig. 6. Distribution of carrier density $N(r)$ for $2a = 2$ μm, $w = 0.4$ μm, and $D = 2$ cm^2/s. Current I is taken as a parameter.

Fig. 6 shows an example of the carrier density distibution $N(r)$. It displays a gradual decrese of the carrier density toward the disk edge due to the diffusion effect. Above threshold, the carrier density near the disk edge is clamped by the stimulated emission. Fig. 7(a) shows the threshold current I_{th} calculated for $2a = 2$ μm, where results obtained with r_1 are converted to w by the relation $r_1 = 1.12w$. The minimum threshold current is 8–20 μA at $w = 0.4$ μm. The threshold is

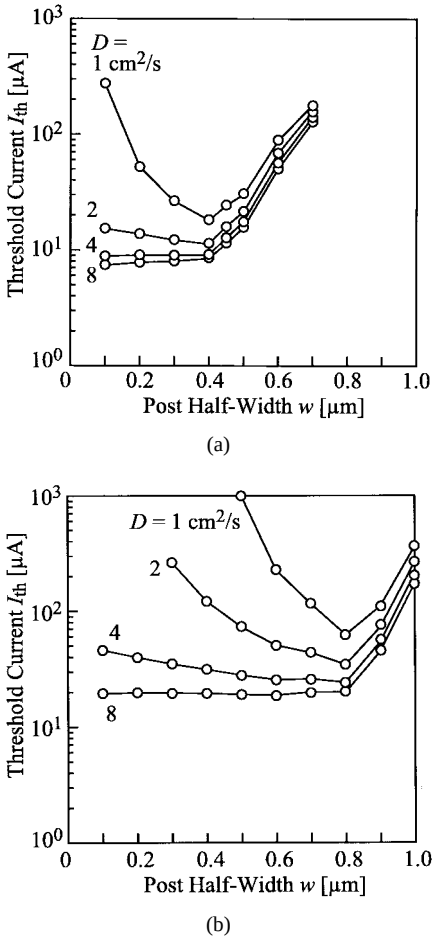

Fig. 7. Threshold current $I_{\rm th}$ calculated with post half-width w for: (a) $2a = 2$ μm and (b) 3 μm. Diffusion constant D is taken as a parameter.

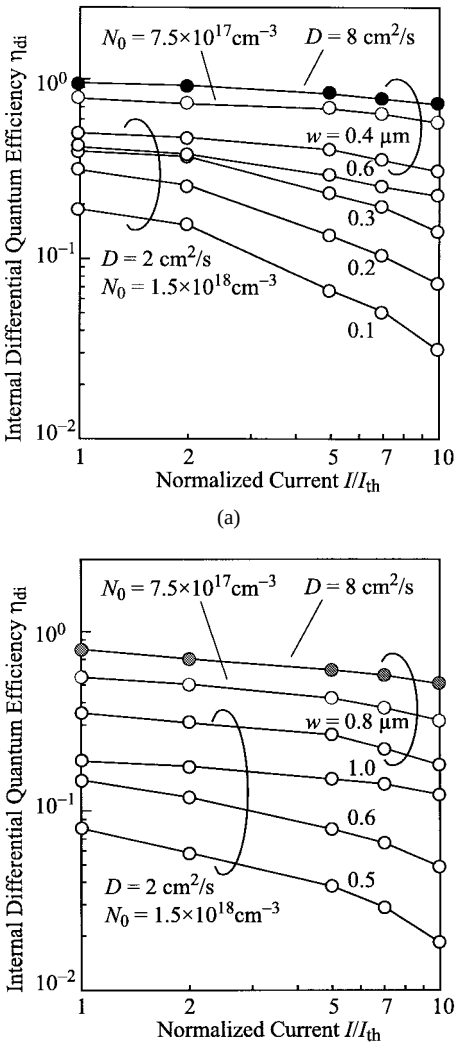

Fig. 8. Internal differential quantum efficiency $\eta_{\rm di}$ calculated with current normalized by threshold current $I/I_{\rm th}$ for: (a) $2a = 2$ μm and (b) 3 μm. Post half-width w, diffusion constant D, and transparent carrier density N_0 are taken as parameters.

increased with the decrease of w from the optimum value due to the insufficient carrier diffusion. It is also increased with the increase of w from the optimum value due to the increase of the scattering loss at posts. Fig. 7(b) shows results for $2a = 3$ μm. The dependence is similar to that for $2a = 2$ μm. The minimum threshold current is 20–80 μA at $w = 0.8$ μm. The optimum w corresponds to the exposed disk width of 0.7 μm. This value is comparable to 0.6 μm for $2a = 2$ μm. These are slightly larger than those just expected from the distribution of WG modes [3].

Fig. 8(a) shows the internal differential quantum efficiency $\eta_{\rm di}$ for $2a = 2$ μm. The efficiency $\eta_{\rm di}$ is decreased for a higher injection current due to the increase of the leakage current passing through Region 1, which is lost as the spontaneous emission coupled to nonlasing modes. Both smaller and larger posts increase the threshold so that the increased Auger recombination as well as the leakage current further reduce $\eta_{\rm di}$. The maximum value at threshold is 50% at $w = 0.4$ μm. This value is lower that the ratio of the area of Region 2 to the total area of the disk, i.e., 80%, and lower than in well-designed stripe lasers. Obviously, it is affected by the nonuniform carrier distribution, as shown in Fig. 6. We investigated the improvement of the low $\eta_{\rm di}$. The increase of the carrier density in Region 1 can be suppressed by reducing the carrier density for the transparency N_0. If N_0 is reduced to 7.5×10^{17} cm^{-3}, $\eta_{\rm di}$ at threshold is improved to 80%. Such a low N_0 is expected in a MQW with n-type delta-doped barrier layers [23]. A larger diffusion constant D also improves $\eta_{\rm di}$; it is 95% for $D = 8$ cm^2/s. This value is unexpectedly high for the ratio of the area of Region 2. It might be attributed to the large diffusion current from Regions 1 to 2, which was enhanced even below threshold by the stimulated emission for the lasing mode having the large spontaneous emission factor. Fig. 8(b) shows results for $2a = 3$ μm. Overall injection levels, the efficiency obtained with the optimum w is about 0.7 times that for $2a = 2$ μm. This is simply due to the increase of the ratio of area of Region 1.

III. Fabrication and Evaluation

The wafer and the fabrication process are fundamentally the same as those described in [13]. The wafer was equipped with the GaInAsP CS-MQW active layer of nearly 0.2 μm in total thickness and four layers of quantum wells. The process flows as the metallization, the electron beam lithography of dot

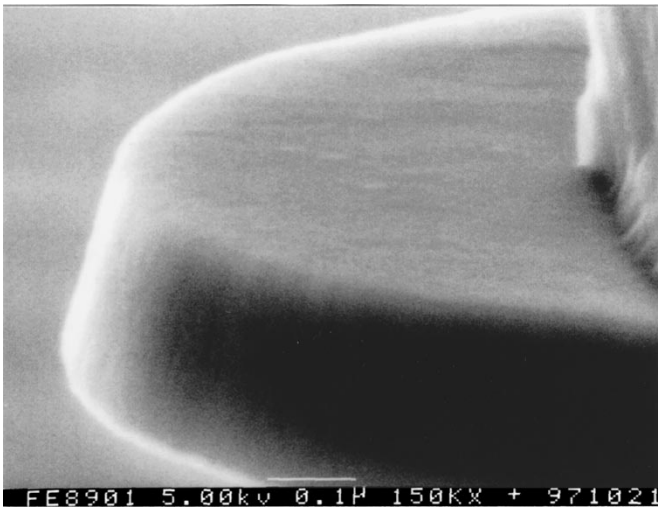

Fig. 9. Magnified view of formed disk edge.

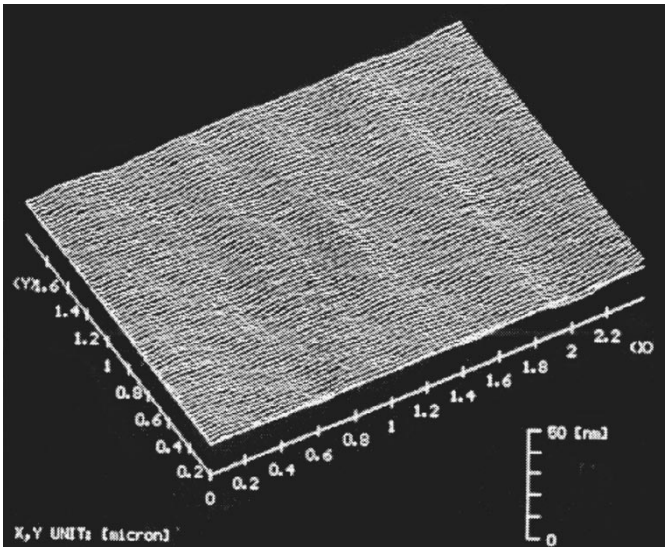

Fig. 10. Topographic image of sidewall etched by methane-based ECR etching.

patterns, the mesa formation by the methane-based electron cyclotron resonance (ECR) plasma etching, the annealing to form the ohmic contact, and the selective wet etching of InP cladding layers to form the disk.

As the improvement of the process, we focused on the condition of the ECR etching. During the ECR etching, flow rates of CH_4, H_2, and Ar were 0.65, 0.9, and 0.3 sccm, respectively, and the total gas pressure was 8×10^{-5} Torr. The microwave power and the acceleration voltage were 100 W and 200 V, respectively. It is often discussed as the advantage of methane-based dry etchings that the polymer deposited during the etching protects the etching mask. In our experiments, however, the excessive polymer caused the roughness at the etched surface and sidewall. In addition, the polymer sometimes disturbed the uniform wet etching of InP claddings layers. This is the reason we used the relatively low gas pressure. In this study, we further made an effort to suppress the polymer deposition by cleaning the etching chamber repeatedly with the O_2 plasma for every half-hour of the etching. Another important improvement that was indicated in the theoretical calculation is the control of the post width. In this experiment, however, we simply controlled the width by the wet etching time. As shown in Section II-B, the optimum etch depth is 0.6–0.7 μm for $2a = 2$–3 μm, respectively. It was obtained by the enchant $HCl:H_2O = 4:1$ at 2 °C with a time denoted as $25a$ [s], where a is in the unit of μm. Even with the optimum etching time, some nonuniformity in etch depth might be introduced by the bubble during the etching. Fig. 9 shows the magnified view of the formed disk edge. The sidewall angle against the disk surface was 80°. The very smooth sidewall and surface are observed, which owes to the improved ECR etching and the high selectivity of the wet etching. Fig. 10 shows the topographic image of the sidewall of the disk. It was observed by a multicannel field emission scanning electron microscope Elionix ERA-8000FE. The maximum and average roughnesses were evaluated to be 8.5 and 0.88 nm, respectively. They are 15% and 19% smaller than those without the chamber cleaning, respectively. The average roughness is almost the same as that of the cleaved facet.

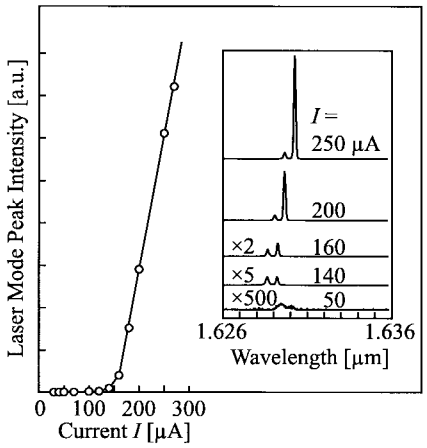

Fig. 11. Laser mode peak intensity versus current characteristic and lasing spectra observed under CW condition at 298 K for 3-μm-diameter device.

In the measurement of lasing characteristics, the current was flowed directly from a sharpened tungsten probe to the top contact. The light radiated from the device was detected by a single mode fiber and analyzed by an optical spectrum analyzer. Fig. 11 shows the peak intensity of the lasing mode for a 3-μm-diameter device. It was observed under CW condition at 298 K with a spectral resolution of 0.1 nm. The threshold current $I_{\rm th}$ was 150 μA. This value is the lowest record ever reported for GaInAsP–InP lasers. If the uniform carrier distribution is assumed, the threshold current density $J_{\rm th}$ is calculated to be 2.1 kA/cm^2. This value includes the leakage current through Region 1. The ratio of the current diffused to Region 2 is calculated to be 26% at the threshold for the optimum post widths. Considering that the lasing mode is localized in Region 2, the effective threshold current density is estimated to be 0.86 or 0.22 kA/cm^2 per well. This value is reasonably low for the achievement of the CW lasing.

In the spectra of Fig. 11, two resonant modes are seen near the wavelength of 1.63 μm. The spectral full-width at half-maximum (FWHM) of the longer wavelength mode reached

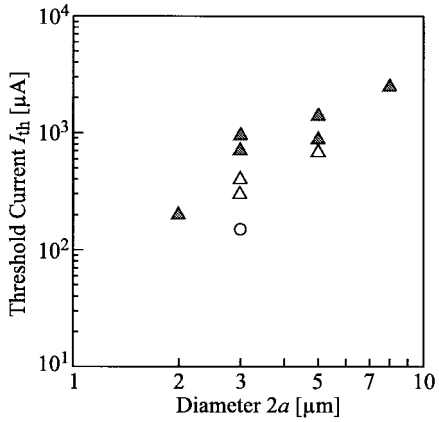

Fig. 12. Dependence of threshold current $I_{\rm th}$ on disk diameter $2a$. Open and closed symbols indicate ECR etching condition with and without chamber cleaning, respectively. Triangular and circular symbols indicate pulsed and CW conditions, respectively.

the resolution limit above threshold. The FWHM of the lasing mode was 0.5 nm for a current less than 50 μA, and that of the nonlasing mode was 0.7 nm. From these values, Q factors were calculated to be 3300 and 2300, respectively. The higher Q gives the total cavity loss of 30 cm^{-1} for the lasing mode. The diffraction loss can be negligible for this device, since the disk diameter 3 μm is nearly twice as large as the diffraction limit at which the diffraction loss rapidly increases to far larger than other losses. The internal absorption loss $\alpha_{\rm a}$ is 5 cm^{-1}, as mentioned in Section II-B. Thus, the total scattering loss $\alpha_{\rm s} + \alpha_{\rm p}$ is 25 cm^{-1}. Fig. 12 shows the dependence of the threshold current $I_{\rm th}$ on the disk diameter $2a$. Under pulsed condition, the lasing has been obtained for a diameter from 2 to 8 μm. The threshold current was simply decreased as the disk diameter was reduced. Closed symbols indicate the ECR etching without the chamber cleaning, while open symbols indicate that with the cleaning. The wet etching condition was almost the same for these devices. It is seen that the threshold reduction was achieved by the cleaning, i.e., by the reduction of the scattering loss $\alpha_{\rm s}$. The variation of the threshold for the same diameter and the same ECR etching condition might be caused by the nonuniform wet etching, i.e., by the difference of the width.

Fig. 13 shows the change of the two resonant wavelengths with the current I. The interval between the wavelengths was 0.6 nm and almost constant. From the observed interval, the relative difference of the equivalent index of modes is estimated to be 0.04%. This indicates that two modes have very close field distributions. The interval between neighboring longitudinal modes, which have almost the same radial distribution but have the different number of nodes, is calculated to be 110 nm for a 3-μm-diameter device by the analysis with the equivalent index approximation [13]. The smallest interval of lateral modes having different radial distributions is calculated to be 10 nm. Even considering the error caused by the simple analysis, these values are still much larger than the observed value 0.6 nm. We considered that it was caused by the dissociation of degenerate WG modes. In general, a WG mode has the degeneracy of the infinite number of standing waves having the same profile and different angular

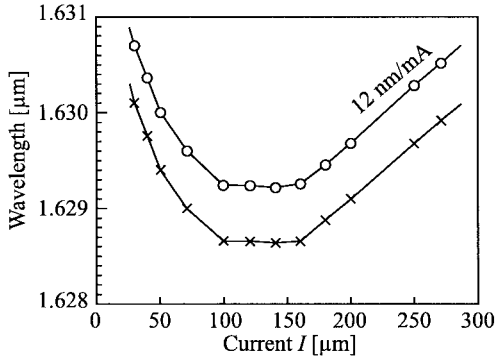

Fig. 13. Wavelength versus current characteristics of CW lasing device. Circle and cross mark denote lasing and nonlasing modes, respectively.

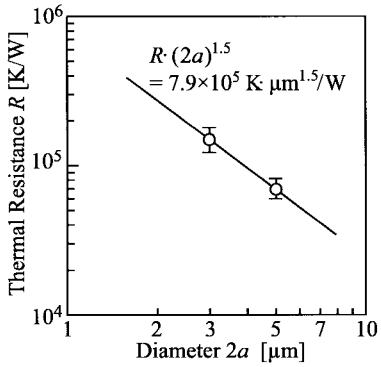

Fig. 14. Dependence of thermal resistance R on disk diameter $2a$.

positions of nodes and antinodes. The degeneracy should be broken by the asymmetry of the fabricated disk. The two modes were considered to satisfy the low loss condition determined by node and antinode positions of standing waves.

As seen in Fig. 13, these modes blue-shifted at lower injection level and red-shifted at higher injection level with the increase of the current. They were caused by the carrier plasma effect and the temperature increase ΔT, respectively. The observed red shift $\Delta\lambda/\Delta I$ was 12 nm/mA, where $\Delta\lambda$ is the wavelength shift and ΔI is the increase of the current. For the GaInAsP–InP system, $\Delta\lambda/\Delta T$ caused by the refractive index change is typically 0.1 nm/K. The thermal resistance R is approximated as $R = \Delta T/(E_{\rm g}\Delta I)$, where $E_{\rm g}$ is the bandgap energy. From these relations, R is calculated to be 1.5 $\times$ 10^5 K/W for $\lambda = 1.63$ μm. This value is the same order as those evaluated previously [3]. This indicates that the thermal resistance is almost independent of the device quality. The dependence of the thermal resistance R on the disk diameter $2a$ was $R \propto (2a)^{-1.5}$, as shown in Fig. 14. The threshold current under CW condition $I_{\rm thcw}$ is empirically expressed as $I_{\rm thcw} = I_{\rm thp}\exp(\Delta T/T_0) = I_{\rm thp}\exp(RE_{\rm g}I_{\rm thcw}/T_0)$, where, $I_{\rm thp}$ is the pulsed threshold current and T_0 is the characteristic temperature. From this equation, the condition required for the CW lasing is expressed as $I_{\rm thp} < T_0/(eRE_{\rm g})$. Assuming $T_0 = 40$ K, critical values of $I_{\rm thp}$ and $I_{\rm thcw}$ are calculated to be 130 and 340 μA, respectively, for a 3-μm-diameter device. The threshold $I_{\rm thcw}$ observed in the experiment satisfies this condition.

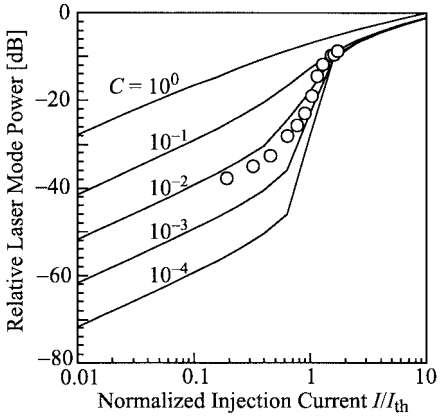

Fig. 15. Log–log plot of laser mode power versus current characteristics and experimental one for CW lasing device.

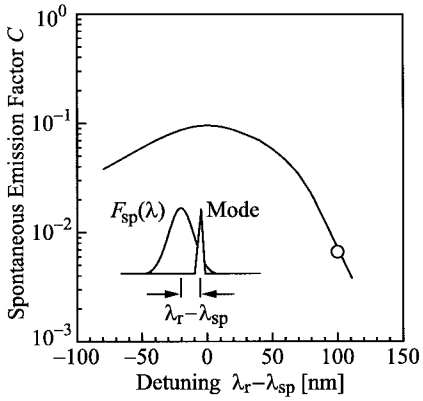

Fig. 16. Dependence of spontaneous emission factor C on detuning of resonant wavelength against spontaneous emission peak $\lambda_r - \lambda_{sp}$. Circle indicates experimental result for CW lasing device.

IV. Spontaneous Emission Factor

The spontaneous emission factor is defined as the coupling efficiency of the spontaneous emission into a lasing mode and is expressed as [3]

$$C = \frac{p\Gamma_r \lambda_{sp}^4 F_{sp}(\lambda_r)}{8\pi n_{eq}^3 V_m} \tag{8}$$

where p is the coefficient denoting the polarization anisotropy of the spontaneous emission, Γ_r the relative confinement factor, $F_{sp}(\lambda)$ the normalized spontaneous emission spectrum, λ_{sp} the center wavelength of the spontaneous emission spectrum, and V_m the mode volume obtained by considering the distribution of the mode standing wave.

The laser mode power versus current characteristic can be calculated against various C factors by the theory in Section II-B. The C factor was estimated by the fitting of theoretical characteristics to the experimental one. Fig. 15 shows the result for the CW lasing device of 3 μm in diameter. Here, the resolution of the optical spectrum analyzer was expanded to 5 nm to measure the laser mode power from the peak intensity. This means that powers of two modes seen in Fig. 11 are intermixed in Fig. 15. The C factor estimated from the fitting was 6×10^{-3}. Fig. 16 shows the dependence of the C factor on the detuning of the resonant wavelength against the spontaneous emission peak, $\lambda_r - \lambda_{sp}$. Here, the theoretical curve was obtained from (8) with the observed spontaneous emission spectrum $F_{sp}(\lambda)$, and the observed polarization anisotropy $p = 1.5$ for the TE polarization of the spontaneous emission from the CS-MQW wafer. The relative confinement factor Γ_r was assumed to be 2. It is typical for the MQW lying near the center of the transverse mode. The mode volume V_m was calculated to be 1.8 μm^3 for the CW lasing device. It is seen in Fig. 16 that C was much reduced by the detuning $\lambda_r - \lambda_{sp}$. It is expected from the mode analysis that the resonant wavelength shifts to 100 nm shorter by reducing the disk diameter to 100 nm smaller. The tuning of the resonant wavelength to the spontaneous emission peak and the reduction of the disk diameter to 1.5 μm will enhance the C factor to 0.31. Furthermore, the C factor will be enhanced to 0.75, the upper limit for the polarized spontaneous emission, if the FWHM of the spontaneous emission spectrum is reduced to 50 nm. Such a narrow spectrum is obtained at low temperature, e.g., 77 K, otherwise at room temperature by introducing (Ga)InAs multiquantum dots [24] for the active region.

V. Conclusion

We have analyzed lasing characteristics of GaInAsP–InP current injection microdisk lasers of 2–3 μm in diameter and found that there exists an optimum post width, related to the scattering loss of the lasing mode and the carrier diffusion. It is the width as the disk is exposed to the air by 0.6–0.7 μm. The threshold current can be 10 μA for the optimized structure with the disk diameter of 2 μm. However, the internal differential quantum efficiency for the lasing mode is limited to nearly 50%. It is mainly due to the leakage current at the center region sandwiched by posts. It can be increased to maximally 95% by reducing the transparent carrier density to 7.5×10^{17} cm^{-3} and enhancing the diffusion constant in the active layer to 8 cm^2/s. In the experiment, we have achieved the room temperature CW operation in a 3-μm-diameter device with a record low threshold of 150 μA. It was mainly owing to the reduction of the threshold current density, which was attributed to the small scattering loss at disk sidewalls reduced by the improved ECR etching. For this device, the spontaneous emission factor was estimated to be 6×10^{-3}. This small value for the small cavity volume was caused by the large detuning of the lasing wavelength against the spontaneous emission peak. The spontaneous emission factor close to 1 and the clearer demonstration of the spontaneous emission control will be realized, if the wavelength tuning is well achieved and the FWHM of the spontaneous emission spectrum is reduced to 50 nm.

Acknowledgment

The authors would like to thank Prof. Y. Kokubun and Prof. Y. Hirose, Yokohama National University, and Prof. K. Iga, Prof. S. Arai, Associate Prof. F. Koyama, and Dr. T. Miyamoto, Tokyo Institute of Technology, for encouragement and discussion. They also wish to thank Dr. A. Kasukawa, The Furukawa Electric Co., Ltd., and Y. Taguchi and H. Suzuki, Elionix Inc., for help with the experiment.

REFERENCES

[1] Y. Yamamoto, S. Machida, K. Igeta, and G. Björk, "Controlled spontaneous emission in microcavity semiconductor lasers," in *Coherence, Amplification, and Quantum Effects in Semiconductor Lasers*, Y. Yamamoto, Ed. New York: Wiley Interscience, 1991, pp. 561–615.

[2] H. Yokoyama and K. Ujihara, Eds., *Spontaneous Emission and Laser Oscillation in Microcavities.* New York: CRC, 1995.

[3] T. Baba, "Photonic crystals and microdisk cavities based on GaInAsP–InP system," *IEEE J. Select. Topics Quantum Electron.*, vol. 3, pp. 808–830, 1997.

[4] S. L. McCall, A. F. J. Levi, R. E. Slusher, S. J. Pearton, and R. A. Logan, "Whispering gallery mode microdisk lasers," *Appl. Phys. Lett.*, vol. 60, pp. 289–291, 1992.

[5] M. Hovinen, J. Ding, A. V. Nurmikko, D. C. Grillo, J. Han, L. He, and R. L. Gunshor, "Blue-green laser emission from ZnSe quantum well microresonators," *Appl. Phys. Lett.*, vol. 63, pp. 3128–3129, 1993.

[6] D. Y. Chu, M. K. Chin, N. J. Sauer, Z. Xu, T. Y. Chang, and S. T. Ho, "1.5-μm InGaAs/InAlGaAs quantum-well microdisk lasers," *IEEE Photon. Technol. Lett.*, vol. 5, pp. 1353–1355, 1993.

[7] U. Mohideen, W. S. Hobson, S. J. Pearton, F. Ren, and R. E. Slusher, "GaAs/AlGaAs microdisk lasers," *Appl. Phys. Lett.*, vol. 64, pp. 1911–1913, 1994.

[8] W. G. Bi, Y. Ma, J. P. Zhang, L. W. Wang, S. T. Ho, and C. W. Tu, "Improvement high-temperature performance of 1.3–1.5-μm InNAsP–InGaAsP quantum-well microdisk lasers," *IEEE Photon. Technol. Lett.*, vol. 9, pp. 1072–1074, 1997.

[9] J. S. Pan, P. H. Cheng, T. D. Lee, Y. Lai, and K. Tai, "0.66 μm InGaP/InGaAlP single quantum well microdisk lasers," *Jpn. J. Appl. Phys.*, vol. 37, pp. L643–L645, 1998.

[10] A. F. J. Levi, S. L. McCall, S. J. Pearton, and R. A. Logan, "Room temperature operation of submicrometer radius disc laser," *Electron. Lett.*, vol. 29, pp. 1666–1667, 1993.

[11] A. F. J. Levi, R. E. Slusher, S. L. McCall, T. Tanbun-Ek, D. L. Coblentz, and S. J. Pearton, "Room temperature operation of microdisk lasers with submilliamp threshold current," *Electron. Lett.*, vol. 28, pp. 1010–1012, 1992.

[12] C. Gmachl, J. Faist, F. Capasso, C. Sirtori, D. L. Sivco, and A. Y. Cho, "Long-wavelength (9.5–11.5 μm) microdisk quantum-cascade lasers," *IEEE J. Quantum Electron.*, vol. 33, pp. 1567–1573, 1997.

[13] T. Baba, M. Fujita, A. Sakai, M. Kihara, and R. Watanabe, "Lasing characteristics of GaInAsP/InP strained quantum-well microdisk injection lasers with diameter of 2–10 μm," *IEEE Photon. Technol. Lett.*, vol. 9, pp. 878–880, 1997.

[14] K. S. Yee, "Numeral solution of initial boundary problem involving Maxwell's equation in isotropic media," *IEEE Trans. Antennas Propagat.*, vol. AP-14, pp. 302–307, 1966.

[15] J. Buus and M. Danielsen, "Carrier diffusion and higher order transversal modes in spectral dynamics of semiconductor laser," *IEEE J. Quantum Electron.*, vol. QE-13, pp. 669–674, 1977.

[16] Y. Suematsu, S. Akiba, and T. Hong, "Measurement of spontaneous-emission factor of AlGaAs double-heterostructure semiconductor lasers," *IEEE J. Quantum Electron.*, vol. QE-13, pp. 596–600, 1977.

[17] G. Mur, "Absorbing boundary conditions for the finite-difference approximation of the time-domain electromagnetic-field equations," *IEEE Trans. Electromagn. Compat.*, vol. EMC-23, pp. 377–382, 1981.

[18] A. Sakai and T. Baba, "FDTD simulation of photonic devices and circuits based on circular and fan-shaped microdisks," *J. Lightwave Technol.*, vol. 17, pp. 1493–1499, Aug. 1998.

[19] W. B. Joyce, "Carrier transport in double-heterostructure active layers," *J. Appl. Phys.*, vol. 53, pp. 7235–7239, 1982.

[20] P. W. A. McIloy, A. Kurobe, and Y. Uematsu, "Analysis and application of theoretical gain curves to the design of multi-quantum-well lasers," *IEEE. J. Quantum Electron.*, vol. QE-21, pp. 1958–1963, 1985.

[21] B. J. Li and P. L. Liu, "Numerical analysis of the whispering gallery modes by the finite-difference time-domain method," *IEEE J. Quantum Electron.*, vol. 32, pp. 1583–1586, 1996.

[22] E. Yablonovitch, T. J. Gmitter, and R. Bhat, "Inhibited and enhanced spontaneous emission from optically thin AlGaAs/GaAs double heterostructure," *Phys. Rev. Lett.*, vol. 61, pp. 2546–2549, 1988.

[23] K. Uomi, "Modulation-doped multi-quantum well (MD-MQW) lasers—I: Theory," *Jpn. J. Appl. Phys.*, vol. 29, pp. 81–87, 1990.

[24] D. L. Huffaker, G. Park, Z. Zou, O. B. Schekin, and D. G. Deppe, "1.3 μm room-temperature GaAs-based quantum-dot laser," *Appl. Phys. Lett.*, vol. 73, pp. 2564–2566, 1998.

Masayuki Fujita was born in Yokohama City, Japan, on November 12, 1974. He received the B.E. and M.E. degrees from the Division of Electrical and Computer Engineering, Yokohama National University, Japan, in 1997 and 1999, respectively. He is presently working toward the Ph.D. degree in the Division of Electrical and Computer Engineering, Yokohama National University, and studying spontaneous emission control in ultrasmall disk lasers.

Mr. Fujita is a member of the Japan Society of Applied Physics.

Atsushi Sakai was born in Saitama Prefecture, Japan, on September 4, 1970. He received the B.E. and M.E. degrees from the Division of Electrical and Computer Engineering, Yokohama National University, Japan, in 1997 and 1999, respectively. He is presently working toward the Ph.D. degree in the Division of Electrical and Computer Engineering, Yokohama National University, and studying FDTD simulation and the fabrication of photonic integrated circuit composed of microdisks.

Mr. Sakai is a member of the Japan Society of Applied Physics.

Toshihiko Baba (M'93) was born in Nagano Prefecture, Japan, on November 12, 1962. He received the B.E., M.E., and Ph.D. degrees from the Division of Electrical and Computer Engineering, Yokohama National University, Japan, in 1985, 1987, and 1990, respectively.

During his Ph.D. work, he was engaged in antiresonant reflecting optical waveguides (ARROW's) and integrated lightwave circuits. In 1990, he joined the Precision and Intelligence Laboratory, Tokyo Institute of Technology, as a Research Associate and started research on vertical-cavity surface-emitting lasers (VCSEL's). In 1991, he reported the first calculation of spontaneous emission factor in VCSEL's. In 1993, he achieved the first RT CW operation of a long wavelength VCSEL. In 1994, he became an Associate Professor at Yokohama National University. He was also a Guest Associate Professor at Tokyo Institute of Technology from 1994 to 1999. His current interests are microcavity lasers, photonic band crystals, spontaneous emission control, micromechanical optics, nonlinear optics, and optical computing.

Dr. Baba is a member of the Institute of Electronics, Information, and Communication Engineers of Japan (IEICE), the Japan Society of Applied Physics, and the American Institute of Physics. He received the Niwa Memorial Prize in 1991, the Best Paper Award of Microoptic Conference in 1993 and 1999, and the Paper Award and the Academic Encouragement Award from the IEICE in 1994.